THE JOURNAL OF PHYSICAL CHEMISTRY B LETTERS

2006, *110,* 9363−9367
Published on Web 04/21/2006

Dynamic Distance Disorder in Proteins Is Caused by Trapping

Guobin Luo,[†,‡] Ioan Andricioaei,[†,§] X. Sunney Xie,[*,†] and Martin Karplus[*,†,∥]

Department of Chemistry and Chemical Biology, Harvard University, Cambridge, Massachusetts 02138, and Institut Le Bel, Université Louis Pasteur, Strasbourg, France

Received: December 23, 2005; In Final Form: March 8, 2006

Dynamic disorder in proteins, as demonstrated by variations in single-molecule electron transfer rates, is investigated by molecular dynamics simulations. The potential of mean force for the fluctuating donor−acceptor distance is calculated for the NAD(P)H:flavin oxidoreductase (Fre) complex with flavin adenine dinucleotide (FAD) and is found to be in agreement with that estimated from electron transfer experiments. The calculated autocorrelation function of the distance fluctuations has a simple exponential behavior at low temperatures and stretched exponential behavior at higher temperatures on femtosecond to nanosecond time scales. This indicates that the calculated dynamic disorder arises from a wide range of trapping times in potential wells on the protein energy landscape and suggests a corresponding origin for the stretched exponential behavior observed experimentally on longer time scales.

Introduction

Conformational dynamics of biomolecules is essential to their functions, as demonstrated by many experimental and theoretical studies.[1] A picture has emerged in which both static heterogeneity (i.e., individual molecules with the same composition have different properties[2]) and dynamic disorder (a given molecule has properties that vary with time[3]) give rise to complex dynamic behavior.[4−6] One of the pioneering experiments on this area was the study of Frauenfelder and co-workers who measured the rebinding kinetics of CO after photodissociation.[2,7] Since spontaneous fluctuations of individual molecules are not synchronized, it is difficult to observe them directly in an ensemble-averaged experiment. However, they were able to observe multiexponential kinetics in an ensemble experiment by using photodissociation to synchronize the behavior of the molecules. The rebinding was found to be complex with a multiexponential time dependence and a non-Arrhenius temperature dependence covering a wide range of temperatures (10−350 K) and time scales (100 ns to ∼1000 s).

Recent advances in room-temperature fluorescence spectroscopy have made possible the real-time observation of single biomolecules,[8,9] thus circumventing the problem of synchronization. Of particular interest are distance-sensitive probes based on fluorescence resonance energy transfer (FRET)[10] or electron transfer (ET),[11] which reveal information on conformational fluctuations. The observed conformational fluctuations of enzymes coincide in time scale with the fluctuations in their catalytic reactivity in some cases.[12,13] Molecular dynamics simulations have been used to complement single-molecule measurements of conformational dynamics related to enzyme activity.[14] In the electron transfer experiments, the measurements were interpreted in terms of distance fluctuations on the Ångström length scale and on the millisecond to second time scale between a fluorescent chromophore and a nearby tyrosine quencher, based on the exponential distance dependence of the ET rate.[15,16] A stretched exponential decay of the distance autocorrelation function was observed and shown to be consistent with an anomalous diffusion-based model;[17,18] recently, a one-dimensional generalized Langevin equation (GLE) with power-law memory kernel was introduced to interpret the result.[19] Also, it has been found in molecular dynamics simulations that stretched-exponential relaxation occurs in the dynamic structure factor of lysozyme and the results can be fitted by a fractional Brownian motion model.[20] Although these formulations provided compact descriptions of the experiments, they do not determine the underlying molecular mechanism that results in the wide distribution of relaxation times. It is the purpose of the present letter to provide such a mechanism, which explains the simulation results and is suggested to extend to the experimental observations of stretched exponential behavior. We note that our analysis of the distance fluctuations per se is not concerned with the details of the electron transfer process and its complexities on short time scales.[21,22]

Two extreme models for the observed dynamic disorder have been suggested (D. Reichman, private communication). In one model, the molecule visits a series of minima (traps) with a range of well depths and barriers. By introduction of an exponential distribution of trapping energies, an analytical solution for this model has been obtained.[23] In the other model, the multiexponential dynamics arises from the multiplicity of conformational pathways projected onto the measured coordinate; this behavior is related to entropic barriers in protein

* Correspondence to be addressed to: Department of Chemistry and Chemical Biology, Harvard University, 12 Oxford Street, Cambridge, MA 02138. xie@chemistry.harvard.edu, marci@tammy.harvard.edu.
† Harvard University.
‡ Current address: Department of Chemistry, Massachusetts Institute of Technology, Cambridge, MA 02139.
§ Current address: Department of Chemistry, University of Michigan, Ann Arbor, MI 48109.
∥ Université Louis Pasteur.

10.1021/jp057497p CCC: $33.50

folding considered by Bicout and Szabo.[24] The two models correspond to a primarily energetic or entropic origin, respectively, for the multiexponential dynamics. Here, we show that the conformational dynamics probed by single-molecule all-atom simulations on the femtosecond to nanosecond time scale contain signatures of the longer time dynamics observed experimentally.[25] Further, it is demonstrated that the multiminimum character of the potential energy surface plays the essential role in the calculated dynamics; i.e., the complex dynamics of the spontaneous fluctuations has an energetic origin.

Simulation Method

All-atom simulations were performed with version 29 of the CHARMM program,[26] using the CHARMM27 parameter set.[27] The complex of NAD(P)H:flavin oxidoreductase (Fre) and flavin adenine dinucleotide (FAD) partially solvated in a TIP3P water sphere with a 25 Å radius was studied. The charges of the FAD molecule were determined by fitting the electrostatic potential from ab initio quantum mechanical calculations. The coordinates of Fre were obtained from the crystal structure of the Fre/riboflavin complex provided by Dr. Niviére (Niviére, private communication). The coordinates of the isoalloxazine ring of FAD were available from the Fre/riboflavin structure, and the rest of the FAD coordinates were constructed on the basis of the internal coordinates determined from the quantum mechanical calculation used for finding the FAD parameters.

The stochastic boundary simulation method was used in the calculation.[28] To improve the electrostatic energy and force calculations, the charges of the 12 residues outside the water sphere were scaled down by a factor,[29] which mimics the effect of solvation. Molecular dynamics was used for all protein atoms and for water molecules inside a 19 Å sphere; outside that radius, the water molecules were treated by Langevin dynamics to mimic the heat bath effect of the surroundings.[28] In the MD simulation, the electrostatic and van der Waals interactions were truncated at 13 Å with a shifting function beginning at 8 Å. During the simulations, the temperature was maintained with a Nosé-Hoover thermostat[30,31] applied to both the solvent and the protein atoms. The SHAKE algorithm was applied to the bonds with hydrogen atoms to allow a 2 fs time step.[32] At 300 K, several trajectories 5 ns in length were calculated after equilibrating the system for 200 ps. The coordinates were saved every 100 fs. Simulation trajectories at lower temperatures (20−250 K) were found to converge in much shorter times, and the simulations were terminated after 100 ps. For these short trajectories, the coordinates were saved every 20 fs.

Results and Discussion

There are three tyrosine residues in Fre, Tyr^{35}, Tyr^{72}, and Tyr^{116}, close to the flavin-binding pocket. Fluorescence lifetime measurements of the wild-type and mutant Fre/flavin complexes showed that electron transfer from the Tyr^{35} to the excited FAD isoalloxazine is responsible for the fluorescence quenching.[11] The average positions of the bound FAD and the three tyrosine residues of the protein are shown in Figure 1A. Trajectories in Figure 1B are the time-dependent center-to-center distances between the three tyrosines and the isoalloxazine obtained from a 5 ns simulation. It is clear that the Tyr^{35} (with an average distance of 7.8 Å) is always nearest to the isoalloxazine. Tyr^{116} is slightly further away (9.4 Å), and Tyr^{72} is the furthest (15.9 Å). Thus, the calculated relative distances (Tyr^{72} > Tyr^{116} > Tyr^{35}) are in accord with the lifetime measurement results and the static X-ray structure.[33]

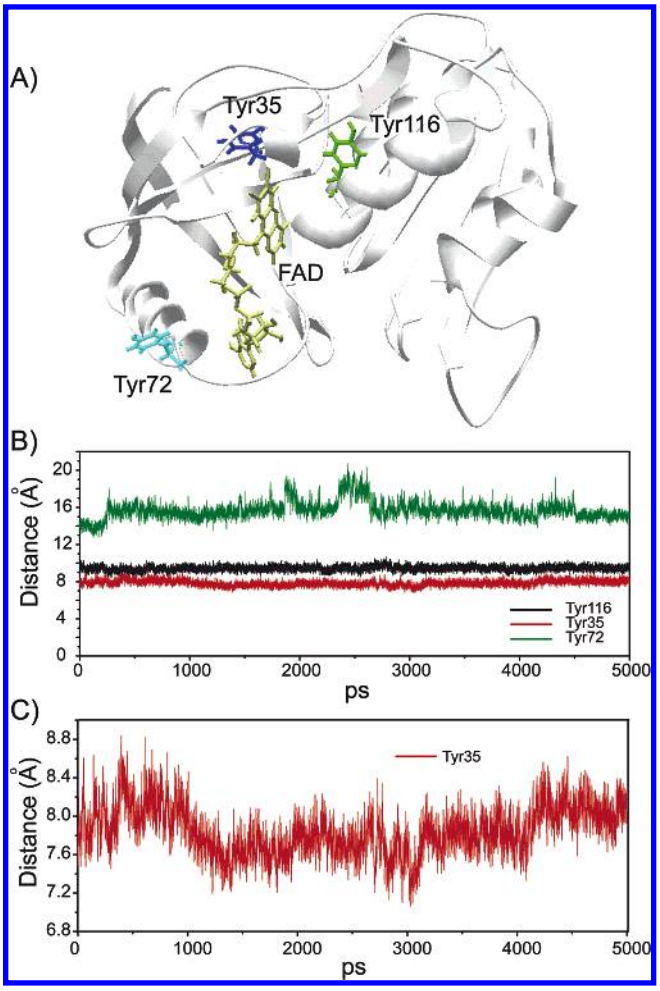

Figure 1. Positions of the tyrosine residues of Fre. (A) The average positions of the three nearby Tyr^{35} (blue), Tyr^{72} (cyan), and Tyr^{116} (green) and the FAD (brown) in a 5 ns simulation. (B) Trajectories of the center-to-center distances between three Tyr residues and the FAD isoalloxazine ring along the 5 ns simulation. (C) The smoothed trajectory of the center-to-center distance between Tyr^{35} and the isoalloxazine, obtained by averaging nine adjacent points from the original trajectory.

Since Tyr^{35} is the major fluorescence quencher, the Tyr^{35}−isoalloxazine distance potential of mean force and the fluctuations of the distance (Figure 1C) are of interest to interpret the experimental data. The potential of mean force (PMF) of the center-to-center distance between the isoalloxazine and the Tyr^{35} was obtained by umbrella sampling;[34−36] trajectories 1 ns in length for each umbrella potential gave converged distributions. Figure 2A shows the statistics of the Tyr^{35}−isoalloxazine distances sampled with different umbrella potentials; the distribution (solid line Figure 2A), which spans a broader distance range, was obtained in a 1 ns simulation without any biasing potential. The Tyr^{35}−isoalloxazine distance PMF resulting from combining these results with the weighted histogram analysis method (WHAM)[34−36] is shown in Figure 2B. The distance distribution has a standard deviation of 0.44 Å. As can be seen from the figure, the calculated PMF is in good agreement with the experimental result.[11] This agreement provides support for the use of the simulations for further analysis. It immediately indicates that the assignment of the fluorescence lifetime fluctuation to the Tyr^{35}−isoalloxazine distance fluctuation is correct. Since the potentials can be approximated by a parabolic function, analytic models of the distance fluctuation have been developed.[17,19]

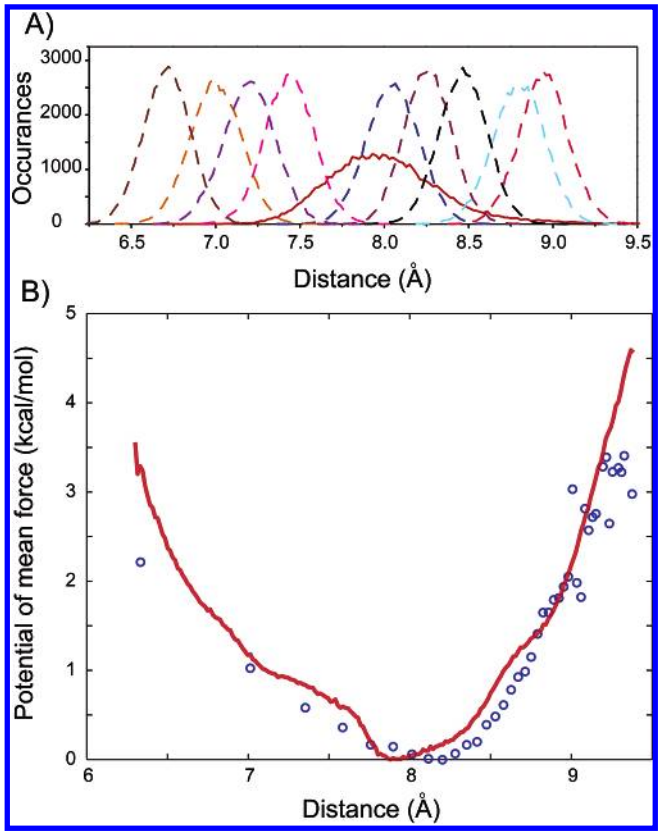

Figure 2. The potential of mean force for the Tyr[35]−isoalloxazine center-to-center distance by umbrella sampling and WHAM. (A) Sampling histograms of the Tyr[35]−isoalloxazine distance under different constraints. Each histogram is obtained from a 1 ns trajectory under different parabolic bias potential applied to the coordinate of Tyr[35]−isoalloxzaine distance. The solid line is the histogram with constraint-free simulation. The dashed lines are histograms with umbrella potential added with a force constant of 20 kcal·Å^{-2} and central positions, from left to right, of 6.6, 6.9, 7.2, 7.4, 8.1, 8.3, 8.6, 8.9, and 9.2 Å. (B) The potential of mean force of the center-to-center distance between Tyr[35] and FAD isoalloxazine, generated with nine constrained and one unconstrained dynamics samples of 1 ns simulations. Also shown is the experimentally obtained potential of mean force (in circles) overlaid with the simulated potential.

The relaxation dynamics of the Tyr[35]−isoalloxazine distance (Figure 1C) can be characterized by the distance autocorrelation function, defined by $C(t) = \langle \delta d(\tau)\ \delta d(\tau + t) \rangle$,[37] where δd is the deviation of distance from its average value and $\langle ... \rangle$ denotes the time average over the trajectory; the un-normalized distance autocorrelation function gives the amplitude and time scale of the distance fluctuations. Figure 3A shows the $C(t)$ obtained from one 5 ns trajectory, whose decay extends over the entire range of the simulation; for times greater than 500 ps, the statistics are such that the results are not meaningful. Results from the other two simulations are similar. The amplitude of the distance fluctuations obtained from the $C(t)$ is on the sub-angstrom scale, consistent with X-ray crystallographic data and estimates from the single-molecule experiments. There are clearly two distinct regimes in the decay of $C(t)$, which correspond to different types of motions. On a time scale of 2 ps, the correlation function shows a rapid decay, as well as a small oscillation; the latter occur in all the trajectories. Figure 3B shows the Tyr[35]−isoalloxazine distance correlation function with higher time resolution obtained from an independent 1 ns simulation trajectory, in which data were recorded at intervals of 20 fs. This part of the correlation function can be fitted by the sum of two independent motions: a fast exponential decay, modeled as Brownian diffusion in a harmonic well; and a slowly decaying oscillation due to a vibrational motion with slight damping[38,39] projected onto the coordinate of Tyr[35]−isoalloxazine distance. The amplitude of the fast decay of the autocorrelation function is about 0.05 Å^2 at 300 K. On the longer time scale, the distance autocorrelation function is highly nonexponential and can be fitted by a stretched exponential $C(t) = C(0) \exp[-(t/\tau)^{\alpha}]$ with the parameters $\alpha = 0.33$ and $\tau = 306$ ps. The correlation function has not fully decayed at the end of the interval accessible from the trajectory. This is in accord with the fact that the standard deviation of the distance of the 5 ns trajectory is only 0.3 Å, less than the estimate of 0.44 Å from the PMF (Figure 2B).

The transition from the short-time Brownian motion to the longer-time subdiffusional motion found in molecular dynamics simulations suggests that the fluctuation on the picosecond to nanosecond time scale and the complex dynamics observed experimentally on a longer time scale have the same origin. It has been found previously by simulations with quenching that the potential energy surface of myoglobin (and probably that of proteins, in general) is a multi-minimum surface with escape times at room temperature ranging from a few tenths of a picosecond to times beyond the length of the simulation.[40,41] Thus, the observed transition in the relaxation described above could originate from a barrier-crossing process in which the system escapes from the potential well in which it exists initially. In this well, the dynamics is simple and can be modeled approximately as the Brownian motion of a harmonic oscillator with a superimposed vibrational motion of the well.[40,39] When the system has enough time to cross over the lowest free energy barrier, it falls into the adjacent potential well. Since there are many local minima on the potential surface with different barrier heights separating the minima, a model of diffusion in a well no longer explains the calculated fluctuation dynamics. Thus, on a long time scale, the overall amplitude of the motion is determined by the potential of mean force, but the dynamics is determined by the rates of barrier-crossing processes.

Molecular dynamics at low temperatures have shown that the atomic fluctuations in a protein are smaller and their magnitudes increase as $T^{1/2}$, as expected from motion in a harmonic well.[40] This suggests that low-temperature simulations should show the simple Brownian decay of the autocorrelation function found at short times at room temperature (Figure 3B). Similar to the earlier results for myoglobin,[40] it was found that, for a series of simulations between 20 and 250 K, a transition occurred at around 200 K, and the fluctuation amplitude had a stronger temperature dependence above that temperature (not shown). Figure 3C shows the Tyr[35]−isoalloxazine distance autocorrelation functions $C(t)$ obtained at the different temperatures. The fast Brownian decay with a similar time scale exists at all different temperatures. Below 200 K, only this fast relaxation is found in most cases, while at 250 K, a slower decay analogous to that at 300 K is clearly seen on the longer time scale; at 150 K, there is a weak long-time decay, suggesting that the molecule was in a shallow well from which it could escape on the simulation time scale. With the increase in temperature, the system has a higher probability of crossing the barriers between potential wells at a finite simulation time (100 ps in our case). This observation provides direct evidence that the complex relaxation dynamics in the simulations originates from the multi-minimum character of the potential surface. Further, the trajectory in Figure 1C shows abrupt jumps of the center-to-center distance, supporting the conclusion that barrier crossing is involved. If the free energy barriers were largely entropic,

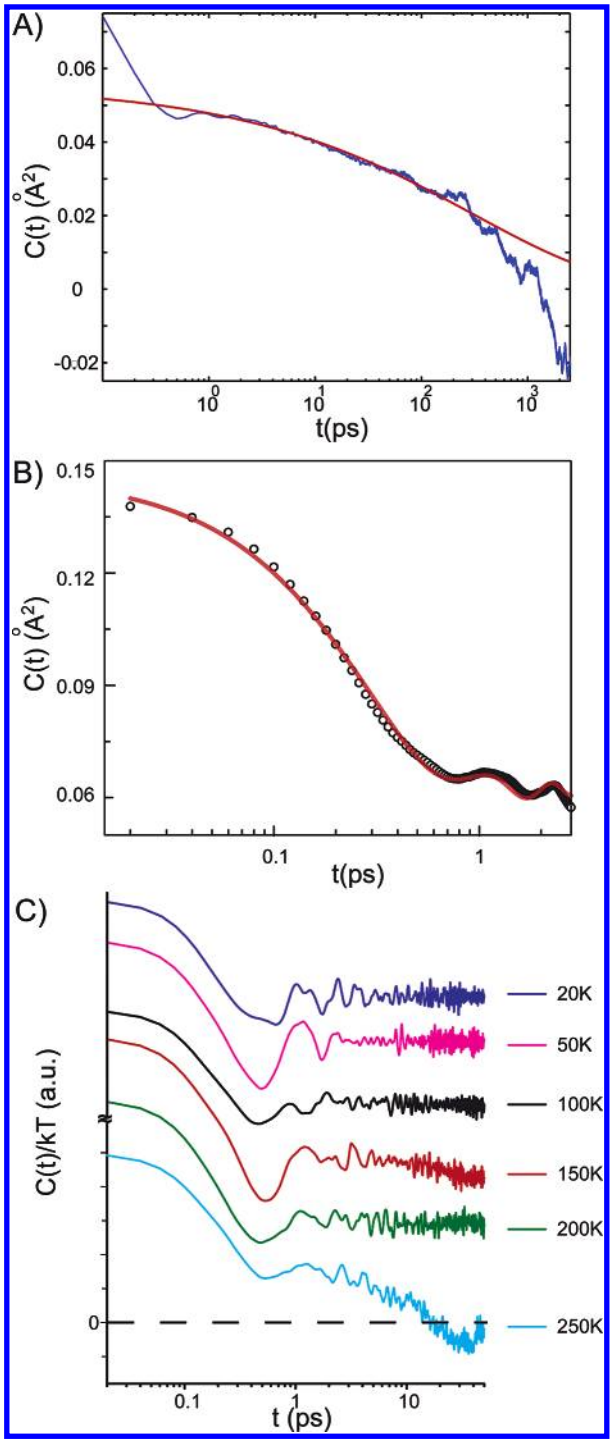

Figure 3. Dynamics of the Tyr[35]−isoalloxazine distance fluctuation. (A) The autocorrelation function (blue) of the Tyr[35]−isoalloxazine distance from the same 5 ns trajectory in Figure 1B, where the decay of the correlation function extends to all the time scales accessible to the simulation. A stretched exponential decay function $C(t) = C(0) \exp[(t/\tau)^{\alpha}]$ (red) is used to make a phenomenological fit to the correlation decay in the 1−500 ps range. The oscillatory behavior at around 1 ps was observed in all the trajectories. (B) The Tyr[35]−isoallozaxine distance autocorrelation function on short time scales at higher time resolution, and a fit with the sum of two independent motions: a Brownian diffusion within a harmonic potential and a vibration with slight damping, $C(t) = A_1 \exp(-t/\tau_1) + A_2 \exp(-t/\tau_2)[\cos(\Omega t) + 1/\tau_2\Omega \sin(\Omega t)] + C_0$, where $\tau_1 = 0.26$ ps, $\tau_2 = 2.8$ ps, and $\Omega = 5.6$ ps^{-1}, $A_1 = 0.08$ Å^2, and $A_2 = 0.004$ Å^2. (C) Distance autocorrelation functions from 100 ps simulation trajectories at different temperatures. The correlation functions at 20, 50, 100, 150, and 200 K are offset for clarity.

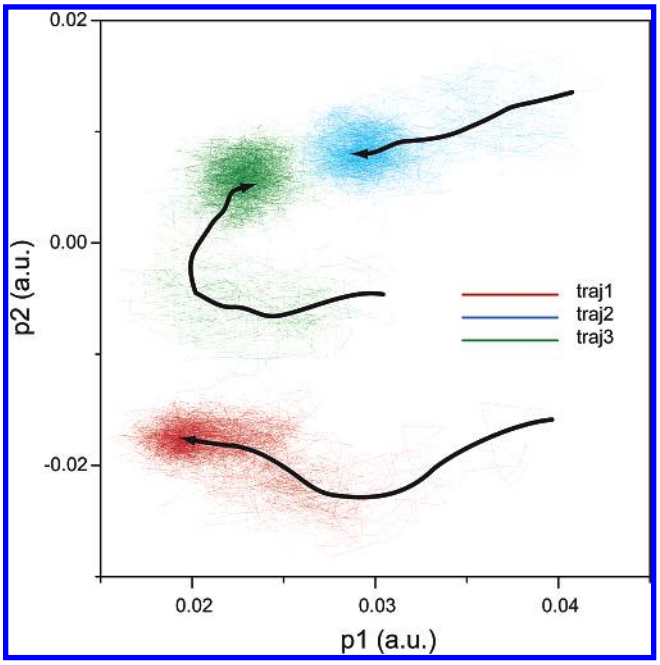

Figure 4. Projection of three 5 ns MD simulation trajectories onto the plane consisting of the first two principal component eigenvectors. Energy minimizations of 1000, 1500, and 2000 steepest descent steps were performed, respectively, from the Fre/FAD complex in the water sphere to generate the initial structure of these three trajectories. State transitions are clearly visible for all three simulations, and different conformational substates are recognized. The black lines outline how the system migrates through different states on the principal plane with time.

the trajectories would be expected to exhibit more gradual drifts in the distance.

Since still-higher barriers that are unlikely to be crossed during the simulation time are expected to exist, as indicated by the PMF, three 5 ns MD trajectories starting from nearly identical initial structures were calculated. They provide additional support for the connection between the nanosecond simulation results and the single-molecule experimental observation of conformational dynamics on the longer time scale. The conformation space explored by the three trajectories is illustrated in Figure 4. A principal component (quasiharmonic) analysis of the Cartesian coordinates of the 232 backbone α-carbon atoms was made.[42,43] It has been demonstrated previously that a small number of principal components account for the major part of the atomic fluctuations and that a series of independent short trajectories provide a better coverage of the accessible configuration space than a single long trajectory.[42] Figure 4 shows the projection of the transient structures onto the first two principal eigenvectors. The two-dimensional projection reveals conformers hidden in a one-dimensional representation. Within the regions sampled by a single trajectory, transitions on the nanosecond time scale from one "well" to another are clearly visible. These contribute to the calculated long-time decay in the distance autocorrelation functions. Further, each of the three trajectories sampled different regions of the conformation space, confirming that the free energy barriers separating them are too high to be crossed on the nanosecond time scale of the simulations. This indicates that longer time scale events contribute to relaxation, in accord with experimental results.

As shown here and observed experimentally, complex relaxation dynamics can occur within a relatively smooth (barrierless) one-dimensional potential of mean force. It is clear that the time dependence of the relaxation dynamics cannot be

deduced from the one-dimensional potential; i.e., the reduction of a multidimensional energy landscape to a single coordinate hide the complexity of the actual potential through integration over essential coordinates.[44] It has been shown here by molecular dynamics simulations that the multi-minimum character of the potential surface gives rise to the multiexponential dynamics. At low temperatures, where the protein is trapped in a single minimum over the time scale of the simulation, Brownian dynamics within that minimum is found from the calculations. As the temperature is raised above 200 K, a long time tail appears in the correlation function due to jumps between wells with different barriers. The existence of high barriers is demonstrated by a principal component analysis of different simulation trajectories. This suggests that the long time character dynamics disorder on a time scale beyond that of the simulation has a corresponding origin. We believe that the existence of dynamic disorder observed in single-molecule experiments and molecular dynamics simulations is a general aspect of biopolymers.

Acknowledgment. The authors thank Dr. Wei Yang for providing the FAD parameters. This work is supported in part by the Department of Energy (S.X.) and the National Institutes of Health (M.K.). The computation was done partly on a 2.4 GHz PC and on a node of a PC cluster at Harvard.

References and Notes

(1) Brooks, C. L., III.; Karplus, M.; Pettitt, B. M. *Proteins: A Theoretical Perspective of Dynamics, Structure, and Thermodynamics*; Advances in Chemical Physics Vol. 71; Wiley-Interscience: Hoboken, New Jersey, 1988.

(2) Austin, R. H.; Beeson, K. W.; Eisenstein, L.; Frauenfelder, H.; Gunsalus, I. C. *Biochemistry* **1975**, *14*, 5355−5373.

(3) Zwanzig, R. *Acc. Chem. Res.* **1990**, *23*, 148−152.

(4) Karplus, M. *J. Phys. Chem. B* **2000**, *104*, 11−27.

(5) Xie, X. S. *J. Chem. Phys.* **2002**, *117*, 11024.

(6) Frauenfelder, H.; Sligar, S. G.; Wolynes, P. G. *Science* **1991**, *254*, 1598−1603.

(7) Steinbach, P. J.; Ansari, A.; Berendzen, J.; Braunstein, D.; Chu, K.; Cowen, B. R.; Ehrenstein, D.; Frauenfelder, H.; Johnson, J. B.; Lamb, D. C.; Luck, S.; Mourant, J. R.; Nienhaus, G. U.; Ormos, P.; Philipp, R.; Xie, A.; Young, R. D. *Biochemistry* **1991**, *30*, 3988−4001.

(8) Xie, X. S.; Trautman, J. K. *Annu. Rev. Phys. Chem.* **1998**, *49*, 441−480.

(9) Weiss, S. *Science* **1999**, *283*, 1676−1683.

(10) Zhuang, X.; Kim, H.; Pereira, M. J. B.; Babcock, H. P.; Walter, N. G.; Chu, S. *Science* **2002**, *296*, 1473−1476.

(11) Yang, H.; Luo, G.; Karnchanaphanurach, P.; Louie, T.-M.; Rech, I.; Cova, S.; Xun, L.; Xie, X. S. *Science* **2003**, *302*, 262−266.

(12) Lu, H. P.; Xun, L.; Xie, X. S. *Science* **1998**, *282*, 1877−1882.

(13) English, B. P.; Min, W.; Oijen, A. M. v.; Lee, K. T.; Luo, G.; Sun, H.; Cherayil, B. J.; Kou, S. C.; Xie, X. S. *Nat. Chem. Biol.* In press.

(14) Chen, Y.; Hu, D.; Vorpagel, E. R.; Lu, H. P. *J. Phys. Chem. B* **2003**, *107*, 7947−7956.

(15) Gray, H. B.; Winkler, J. R. *Annu. Rev. Biochem.* **1996**, *35*, 537−561.

(16) Moser, C. C.; Keske, J. M.; Warncke, K.; Farid, R. S.; Dutton, P. L. *Nature (London)* **1992**, *355*, 796−802.

(17) Metzler, R.; Barkai, E.; Klafter, J. *Phys. Rev. Lett.* **1999**, *82*, 3563−3567.

(18) Metzler, R.; Klafter, J. *Phys. Rep.* **2000**, *339*, 1−77.

(19) Kou, S. C.; Xie, X. S. *Phys. Rev. Lett.* **2004**, *93*, 180603/1−180603/4.

(20) Kneller, G. R.; Hinsen, K. *J. Chem. Phys.* **2004**, *121*, 10278−10283.

(21) Xu, D.; Schulten, K. *Chem. Phys.* **1994**, *182*, 91−117.

(22) McMahon, B. H.; Muller, J. D.; Wraight, C. A.; Nienhaus, G. U. *Biophys. J.* **1998**, *74*, 2567−2587.

(23) Monthus, C.; Bouchaud, J.-P. *J. Phys. A: Math. Gen.* **1996**, *29*, 3847−3869.

(24) Bicout, D.; Szabo, A. *Protein Sci.* **2000**, *9*, 452−465.

(25) Kuczera, K.; Lambry, J. C.; Martin, J. L.; Karplus, M. *Proc. Natl. Acad. Sci. U.S.A.* **1993**, *90*, 5805−5807.

(26) Brooks, B. R.; Bruccoleri, R. E.; Olafson, B. D.; States, D. J.; Swaminathan, S.; Karplus, M. *J. Comput. Chem.* **1983**, *4*, 187−217.

(27) MacKerell, A. D., Jr.; Bashford, D.; Bellott, R. L.; Dunbrack, R. L., Jr.; Evanseck, J. D.; Field, M. J.; Fischer, S.; Gao, J.; Guo, H.; Ha, S.; Joseph-McCarthy, D.; Kuchnir, L.; Kuczera, K.; Lau, F. T. K.; Mattos, C.; Michnick, S.; Ngo, T.; Nguyen, D. T.; Prodhom, B.; Reiher, W. E., III; Roux, B.; Schlenkrich, M.; Smith, J. C.; Stote, R.; Straub, J.; Watanabe, M.; Wiorkiewicz-Kuczera, J.; Yin, D.; Karplus, M. *J. Phys. Chem. B* **1998**, *102*, 3586−3616.

(28) Brooks, C. L., III.; Karplus, M. *J. Chem. Phys.* **1983**, *79*, 6312−6325.

(29) Archontis, G.; Simonson, T.; Karplus, M. *J. Mol. Biol.* **2001**, *306*, 307−327.

(30) Nosé, S. *J. Chem. Phys.* **1984**, *81*, 511−519.

(31) Hoover, W. G. *Phys. Rev. A* **1985**, *31*, 1695.

(32) Ryckaert, J. P.; Ciccotti, G.; Berendsen, H. J. C. *J. Comput. Phys.* **1977**, *23*, 327−341.

(33) Ingelman, M.; Ramaswamy, S.; Niviere, V.; Fontecave, M.; Eklund, H. *Biochemistry* **1999**, *38*, 7040−7049.

(34) Kumar, S.; Bouzida, D.; Swendsen, R. H.; Kollman, P. A.; Rosenberg, J. M. *J. Comput. Chem.* **1992**, *13*.

(35) Boczko, E. M.; Brooks, C. L., III. *J. Phys. Chem.* **1993**, *97*, 4509−4513.

(36) Souaille, M.; Roux, B. *Comput. Phys. Comm.* **2001**, *135*, 40−57.

(37) Yang, H.; Xie, X. S. *J. Chem. Phys.* **2002**, *117*, 10965−10979.

(38) Swaminathan, S.; Ichiye, T.; Van Gunsteren, W.; Karplus, M. *Biochemistry* **1982**, *21*, 5230−5241.

(39) McCammon, J. A.; Wolynes, P. G.; Karplus, M. *Biochemistry* **1979**, *18*, 927−942.

(40) Kuczera, K.; Kuriyan, J.; Karplus, M. *J. Mol. Biol.* **1990**, *213*, 351−373.

(41) Elber, R.; Karplus, M. *Science* **1987**, *235*, 318−321.

(42) Caves, L. S.; Evanseck, J. D.; Karplus, M. *Protein Sci.* **1998**, *7*, 649−666.

(43) Andrews, B. K.; Romo, T.; Clarage, J. B.; Pettitt, B. M.; Phillips, J.; George, N. *Structure* **1998**, *6*, 587−594.

(44) Krivov, S. V.; Karplus, M. *Proc. Natl. Acad. Sci. U.S.A.* **2004**, *101*, 14766−14770.